RESEARCH

KEPCO Journal on Electric Power and Energy
p-ISSN 2465-8111, e-ISSN 2466-0124
Volume 7, Number 1, June 2021, pp. 129-135
DOI 10.18770/KEPCO.2021.07.01.129

Characterization and Mechanical Properties of Stainless Steel 316L Fabricated Using Additive Manufacturing Processes

적층식 제조 공정을 활용한 스테인레스 316L 제작기술의 특징과 기계적 속성

Cheol Choi, Mihee Jung

Abstract

Recently, additive manufacturing (AM) technology such as powder bed fusion (PBF) and directed energy deposition (DED) are actively attempted as consumers' needs for parts with complex shapes and expensive materials. In the present work, the effect of processing parameters on the mechanical properties of 316L stainless steel coupons fabricated by PBF and DED AM technology was investigated. Three major mechanical tests, including tension, impact, and fatigue, were performed on coupons extracted from the standard components at angles of 0, 45, 90 degrees for the build layers, and compared with those of investment casting and commercial wrought products. Austenitic 316L stainless steel additively manufactured have been well known to be generally stronger but highly vulnerable to impact and lack in elongation compared to casting and wrought materials. The process-induced pore density has been proved the most critical factor in determining the mechanical properties of AM-built metal parts. Therefore, it was strongly recommended to reduce those lack of fusion defects as much as possible by carefully control the energy density of the laser. For example, under the high energy density conditions, PBF-built parts showed 46% higher tensile strength but more than 75% lower impact strength than the wrought products. However, by optimizing the energy density of the laser of the metal AM system, it has been confirmed that it is possible to manufacture metal parts that can satisfy both strength and ductility, and thus it is expected to be actively applied in the field of electric power section soon.

Keywords: *Additive Manufacturing, 3D Printing, 316L Stainless Steel, Powder Bed Fusion, Directed Energy Deposition*

I. Introduction

Additive manufacturing (AM), also known as 3D printing, has been considered a promising technology that is well-suited for aerospace, defense applications, and producing medical parts [1][2]. This is mainly due to the distinct advantages compared to the conventional 'subtractive' manufacturing processes such as casting and wrought, including the ability to fabricate complex geometries, improved manufacturing efficiency, and reduced production time [3][4]. Moreover, the AM processes allow fabricating materials with characteristic microstructures and mechanical properties due to the complex thermal history of rapid heating and cooling. With these apparent advantages, AM has newly attracted strong attention for manufacturing electric power or energy-related components.

Although there are several types of metal AM processes, most can be classified into two classes: powder bed fusion (PBF) and directed energy deposition (DED) process [5][6]. Both processes use a laser or electron beam as a thermal source to fuse metallic particles. PBF machines selectively melt a thin layer of metallic powder in a reservoir following 2D scanning paths of a 3D object and suitable for manufacturing very delicate small parts. In contrast, DED has a coaxial nozzle that delivers metal powder (or wire), and a concentrated energy source into the molten pool generated simultaneously. It has a unique ability to fabricate functionally graded metal components and repair valuable parts that cannot be repaired by other traditional methods. Besides, DED is used to fabricate large structures that would be almost impossible to build using PBF techniques. All process parameters must be tuned accurately to achieve a uniform and sound microstructure because AM components are primarily influenced by laser power, beam size, scanning speed, and powder feed rate. It has been shown that the metal AM parts' mechanical properties are comparable to the conventionally manufactured parts [7]-[9]. However, electric power applications require a higher degree of part quality assurance and process reliability that are difficult to achieve by a non-expert.

Several problems, such as anisotropic properties, microstructural defects, and poor ductility, should be solved in advance to apply AM technology into the electric power sector successfully. Because AM components have characteristics of heterogeneous and anisotropic microstructure, resulting in mechanical properties are considerably different from those of wrought commercial counterparts. Additionally, gas entrapment pores and lack of fusion defects are frequently formed during AM processes, which can be detrimental to the mechanical properties of the components [10]-[13]. The current study focused on the characterization of mechanical and microstructural properties of

Article Information

Manuscript Received August 06, 2020, Accepted September 28, 2020, Published online June 30, 2021

The Authors are with KEPCO Research Institute, Korea Electric Power Corporation, 105 Munji-ro Yuseong-gu, Daejeon 34056, Republic of Korea.

Correspondence Author: *Cheol Choi* (*ironguy.cc@kepco.co.kr*)

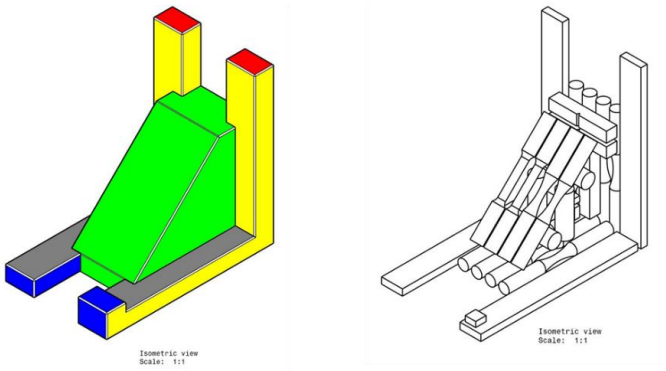

Fig. 1. The shape of standard components for the sampling of microstructure and mechanical test specimens.

316L stainless steel coupons fabricated by PBF and DED.

An attempt was made through the comparative evaluation with conventional manufacturing processes to explain the process-microstructure-property correlation for 316L stainless steel alloy by direct laser deposition.

II. Experimental

A. Material and Additive Manufacturing Processing

Two different kinds of metal AM (PBF, DED) and investment casting processes were used to fabricate 173 mm long × 105 mm wide × 160 mm tall standard components from pre-alloyed stainless steel 316L of complex shapes as shown schematically in the Fig. 1. The standard components were designed to have complex shapes that were appropriately mixed with thin and thick parts to induce a unique microstructure by controlling the cooling speed. Tensile, impact, and high-cycle fatigue test specimens at an angle of 0°, 45°, and 90° relative to the build direction were prepared to study the anisotropic behavior of the buildups.

Two PBF systems (ProX 320 of 3D Systems, SLM 280HL of SLM Solutions) and a DED equipment (MX-Lab of INSSTEK) were used to fabricate the standard components. Besides, investment casting components were also fabricated by Korea Lost-Wax Co., Ltd., and the Ceramic 3D printer (VX500 of Voxeljet) was used to produce wax patterns for casting mold. Because the same standard components could not be made with a commercial wrought process, mechanical test specimens for comparative evaluation were prepared using a forged round bar. In the case of PBF, the energy density was divided into two conditions, 62 J/mm^3 and 87 J/mm^3, to investigate the effects of energy density.

The standard components were subjected to three stages of homogenized heat treatment (650°C / 1.5 hrs + 850°C / 1.5 hrs + 1,040°C / 3 hrs) to remove residual thermal stress during laser deposition. All of the mechanical test specimens were produced according to the ASTM specifications, as shown in Fig. 1.

B. Mechanical Property Tests

MTS Landmark hydraulic equipment (Tension Speed 0.025 mm/s, Fatigue Stress 165±135 MPa, Fatigue Frequency 10 Hz), and the sharpy impact tester were used to evaluate three different mechanical properties at room temperature. The specimens were chemically etched in a solution of (HCl: HNO_3=3:1) for 40 seconds,

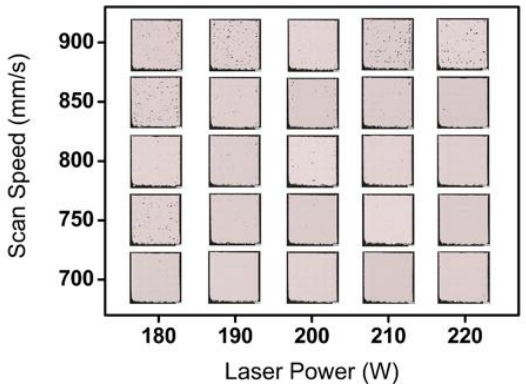

(a)

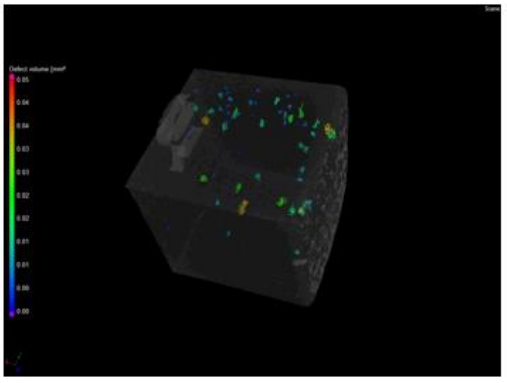

(b)

Fig. 2. Changes in internal defects according to metal AM process parameters. (a) Optical microscope photographs. (b) CT photographs.

and the microstructure was examined by using an optical microscope (Leica, 5000M) and scanning electron microscope (JEOL, 200 kV). Electron backscatter diffraction (EBSD) was also used to characterize the grain structure and compare the grain size of the specimens.

III. Results and Discussion

A. Effect of Processing Parameters

For the direct laser deposition AM process, laser power and scanning speed have been considered as the most critical parameters for buildups' microstructure and mechanical properties. Fig. 2 shows the cube-shaped coupons with a side length of 10 mm by PBF system (SLM280HL of SLM Solutions) combined with deposition parameters (power: 180~220 W, speed: 700~900 mm/min, energy density: 55.55~87.30 J/mm^3). The primary goal of the experiments' design was to optimize laser deposition parameters for producing samples with minimum porosity. The microstructure was examined using a CT scanner to investigate the effect of the two significant parameters on the pore density inside the sample. It can be seen from Fig. 2 that the lowest pore density was observed in the sample that was produced with maximum power (220 W) and minimum scanning speed (700 mm/s). In the figure, the more laser power increases, the slower the scan speed, the lower the volume of defects within the sample. These defects are

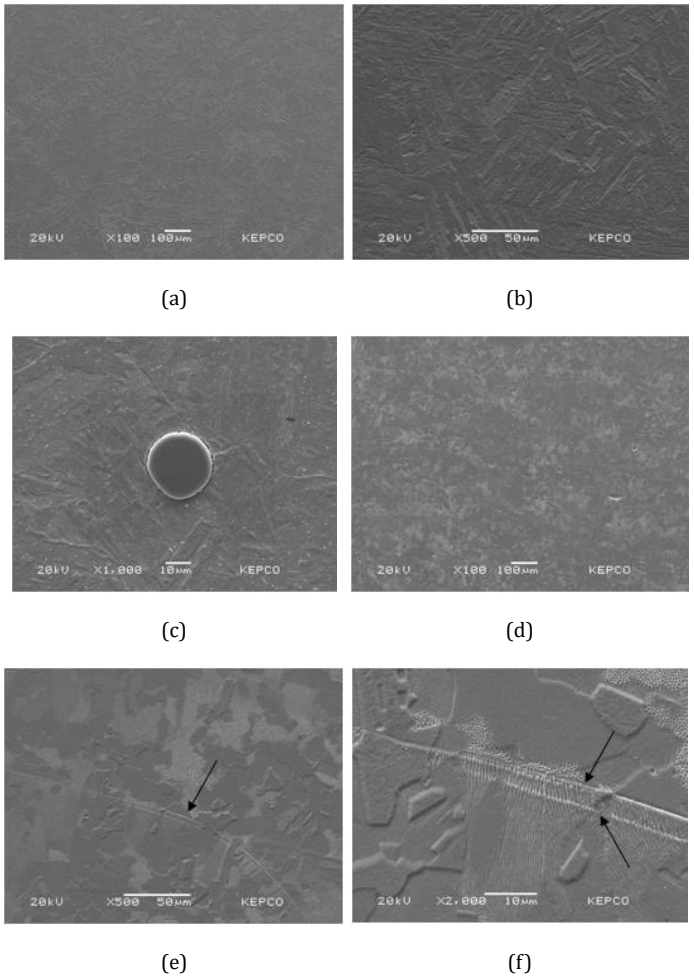

(a) (b)

(c) (d)

(e) (f)

Fig. 3. SEM images of the 316L stainless steel samples produced by PBF process; (a)-(c) high ED PBF, (d)-(f) low ED PBF. Arrows point to the melt pool boundary.

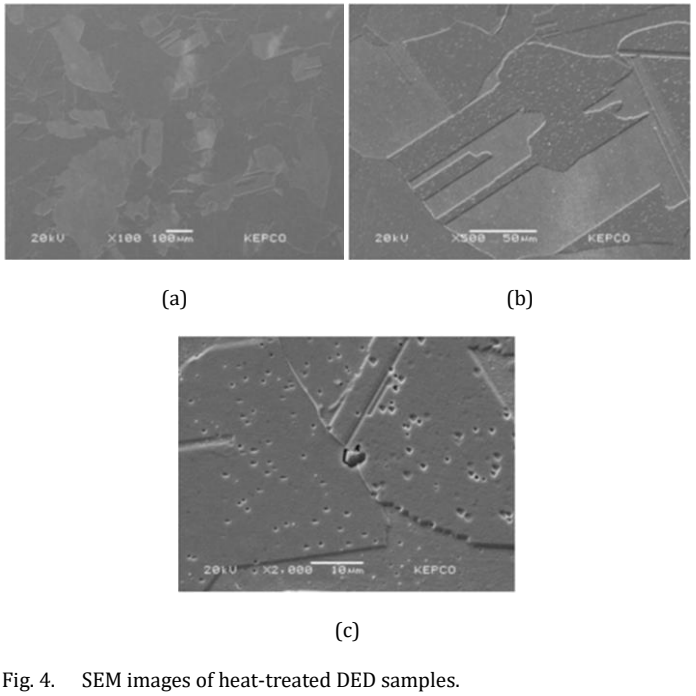

(a) (b)

(c)

Fig. 4. SEM images of heat-treated DED samples.

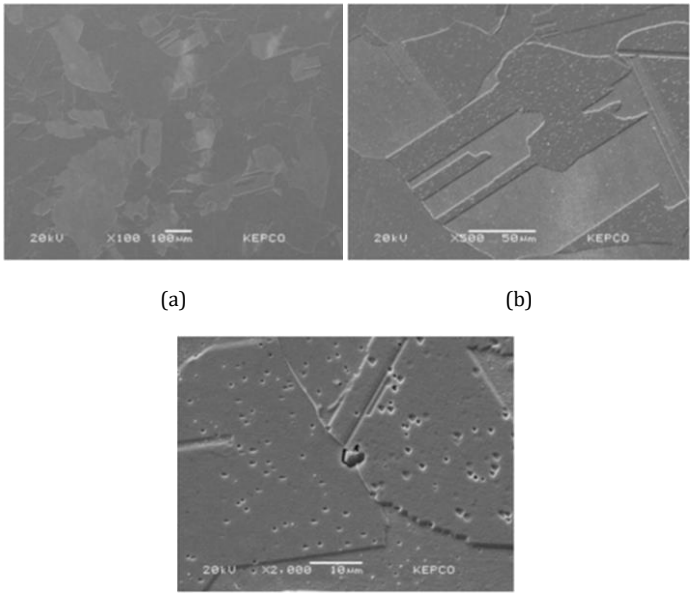

(a) (b)

(c)

Fig. 5. SEM images of conventional manufacturing processes; (a) and (b) As-cast, (c) and (d) Wrought.

attributed to the incomplete melting of metal powder due to a lack of energy. Therefore, laser energy density is considered as a crucial factor that quantifies the energy input that affects the final part's microstructure and mechanical properties in the AM process. In order to investigate the effects of energy density (ED) more closely, standard components were prepared by dividing into two types of PBF process: high energy density (87 J/mm^3) and low energy density (62 J/mm^3). The ProX 320 model of 3D Systems was used to fabricate high ED PBF specimens.

B. Microstructure Characterization

Stainless steel 316L may show very different microstructures depending on the manufacturing process, thus leading to distinct mechanical and physical properties [14]. The microstructures of standard components manufactured by AM processes are shown in Fig. 3 and Fig. 4 compared to those of casting and wrought specimens (Fig. 5). As-cast 316L samples show a relatively coarse columnar grain, so the distance between the dendrite was quite wide. Discrete carbides and incomplete melt defects preferentially along the interdendritic region and pore sizes of 30 to 40 nm are observed depending on the area. Furthermore, in wrought samples, the deformed martensite microstructure characterized by mechanical twin is observed in the grain of the austenite, with no apparent pores being observed, showing a very fine and sound microstructure. In addition, spherical precipitate within 3μm, which are identified as carbides, are also observed over the entire area.

On the other hand, the microstructure of high ED (87 J/mm^3) PBF samples showed a poorly defined, very dense martensitic structure where the shape of the grain is very anisotropic and irregular, with scattered precipitate particles distributing in lath martensite and retained austenite (Fig. 6). Microscopic carbides ranging from several to tens of nm in size throughout the microstructure and rather large carbides with high Si content were

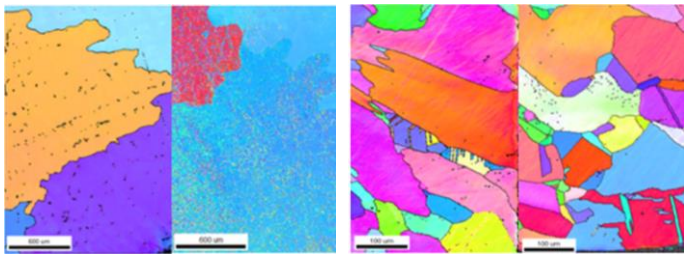

(a) (b)

(c)

Fig. 6. EBSD IPF micrographs of three different processed stainless steel 316L samples; (a) As-cast, (b) DED, (c) high ED PBF.

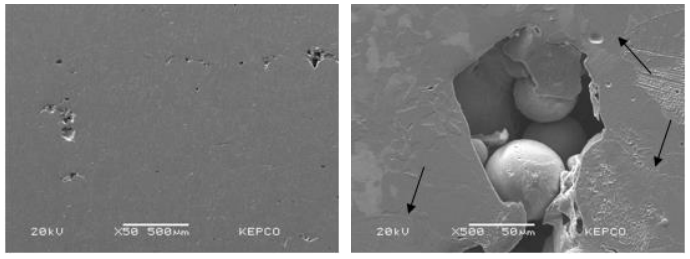

(a) (b)

Fig. 7. Lack of fusion defects observed for low energy density (ED) PBF samples. Arrows point to the melt pool boundary.

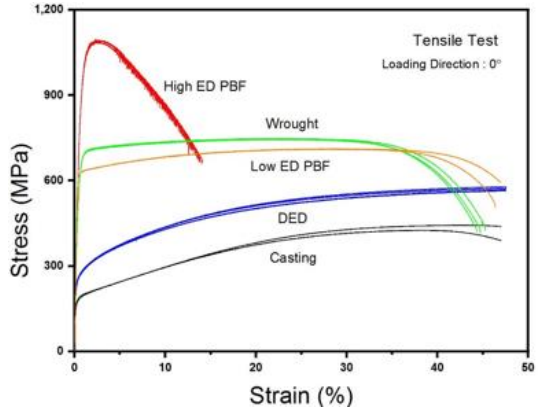

(a)

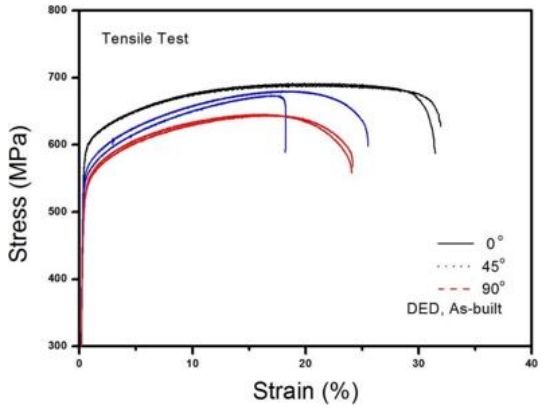

(b)

Fig. 8. Tensile stress-strain curves for five different manufacturing methods after heat treatment(a), and DED specimens in as-built condition(b).

occasionally observed. These fine precipitates may improve the mechanical properties of PBF coupons as compared with conventionally manufactured buildups. The high ED PBF samples' grain size was much smaller than that of the as-cast counterparts due to the rapid cooling rate during the manufacturing process. As a consequence, if PBF process conditions are optimized, it can be confirmed that refined microstructure without coarse defects can be obtained as can be seen in the wrought counterparts.

In contrast, low ED (62 J/mm^3) PBF coupons showed the melt track morphologies clearly in the as-built state. Even after the heat treatment, the melt pool boundary did not disappear completely, but some vague traces of boundary remained, as indicated in Fig. 3(e) and 3(f). Moreover, it is characteristic that the subgranular cellular structures were found locally. Unlike the PBF samples, the DED coupons showed a recrystallized (equiaxed) microstructure after heat treatment, and no melt pool boundary was visible (Fig. 4). However, a uniform distribution of oxides measuring tens of nm across the grain was observed, and some void or cracks surrounding inclusions mainly occurred around the grain boundary.

Low ED process may produce a melt pool too small to sufficient overlap with neighboring melt pools, and thus, many defects were observed contrasted to the high ED samples [15]. Especially when there is a possibility of particle surface oxidation due to a problem in the storage of metal nanopowder, various and large amounts of porosity were observed in the manufactured parts. These pores were irregularly shaped and typically larger (100 μm~400 μm in length) than the spherical pores found. In some cases, the metal powder, which is not completely melted, was observed in pores (Fig. 7), indicating that the energy needed to fuse the powder was insufficient. In particular, those lack of fusion defects strongly depended on the workers and environments, even with the same equipment, materials, and process conditions. These results are thought to be mainly due to the problem of surface oxidation in metal powder during the storage or handling of nano-scale ultra-fine particles.

C. Mechanical Properties

In Fig. 8(a), tensile stress-strain curves of the AM samples after solution heat treatment are shown along with the curves taken from the reference as-cast and wrought samples. The high ED PBF specimens show the highest ultimate tensile strength (1,090 MPa, UTS) and yield strength (820 MPa, YS), which are 39-46% higher than those measured for reference wrought specimens, which consistent 747 MPa and 590 MPa, respectively. Besides, after reaching the UTS, the strength tended to decrease significantly due to the non-uniform and local plastic deformation and decreased to

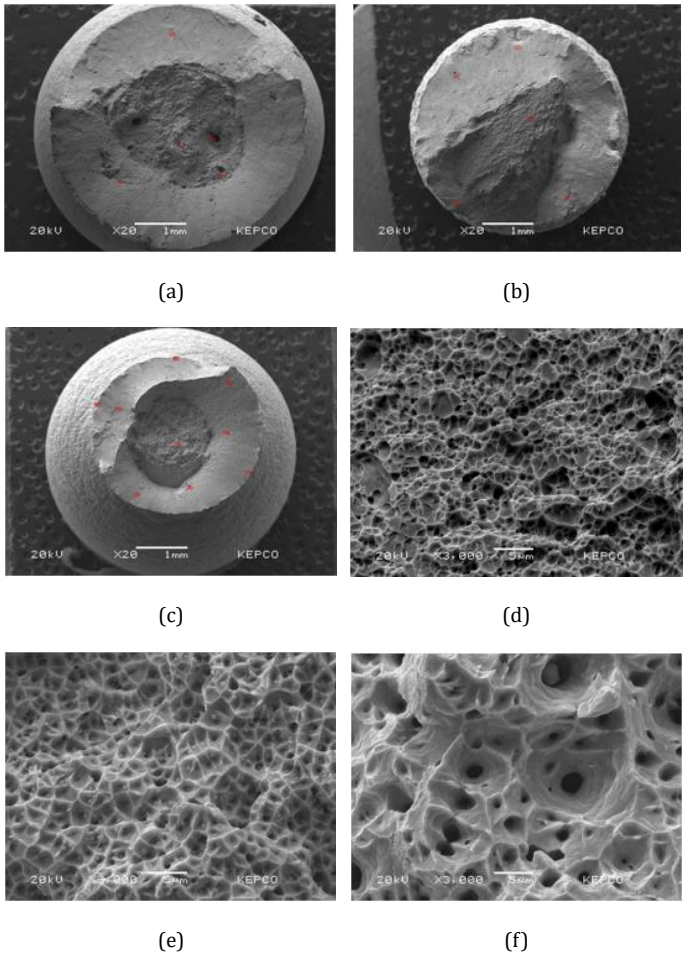

Fig. 9. SEM fractographs of the 316L SS samples after tensile test after heat treatment; (a) and (d) high ED PBF, (b) and (e) DED, (c) and (f) wrought specimen.

the level of 700MPa just before breaking. It was found that the strain to failure (14%) did not reach the desired level, which is much lower than that of the wrought samples (45%). As is generally known, defects and porosity may reduce the apparent strength and ductility at the same time [15]. However, because the high ED PBF samples show the highest strength, it is reasonable to think that the lower ductility is mainly attributed to the hard and brittle martensitic phase formed during the rapid solidification process. Interestingly, the high ED PBF samples did not show any anisotropic tensile properties regardless of heat treatment.

In contrast, the as-built DED specimens showed a much lower strength than the high ED PBF samples, and the difference between UTS and YS was significantly reduced. In particular, it displayed anisotropic tensile properties with high strength and elongation in the order of 0° > 45° > 90° inclination of deposition layers to the loading direction. That is, the strength (UTS: 690 MPa, YS: 585 MPa) and elongation rate (EL: 32%) were higher in a loading direction parallel to the laminated plane, but both the strength (UTS: 645 MPa, YS: 521 MPa) and the elongation rate (EL: 24%) were the lowest in a direction perpendicular to the plane. The EL of 24% is the lowest value for the DED samples in the as-built state, but it is worth noting that it is almost twice as high as one of the high ED PBF samples.

Unexpectedly, the homogenized heat treatment did not seem to have much effect on tensile properties in most specimens. However, it was able to confirm that the tensile properties of the DED samples,

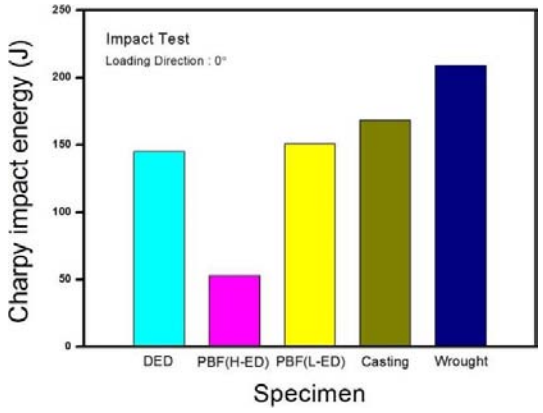

Fig. 10. Comparison of the impact energy for 316L SS specimens taken from the standard components after heat treatment.

which showed anisotropic properties in the as-built condition, were significantly changed by heat treatment. For all DED specimens, the material deviation from the anisotropy was disappeared, and the strength (UTS: 573 MPa, YS: 248 MPa) decreased slightly, while the ductility increased significantly, resulting in no fractures within the strain gauge's operating range (~48%). Moreover, no local necking phenomenon occurred, resulting in breakage under maximum load conditions. Finally, for as-cast specimens, the lowest level of strength (UTS: 420 MPa, YS: 174 MPa) and good ductility (EL of 40%) were observed.

In summary, samples manufactured using the AM process tend to be extremely strong while the elongation rate is insufficient, or if the elongation rate is adjusted through post-heat treatment, the strength tends to decrease significantly. This behavior is thought to be adjustable as much as possible by optimizing heat treatment or AM process conditions. Thus, PBF specimens with reduced energy density were also processed, and tensile tests were conducted, resulting in a balance of strength (UTS: 713 MPa, YS: 618 MPa) and ductility (EL>48%), as shown in Fig. 8(a). This value corresponds to excellent tensile properties comparable to the wrought samples.

The high ED PBF specimens showed a deficient elongation rate, so the fracture behavior was expected to show a brittle style rather than ductile, but it showed typical cup-and-cone ductile fracture patterns, as shown in Fig. 9(a) and 9(d). Interestingly, this was the same for wrought samples with good ductility, and the only difference was the dimple's size can be seen in the fracture surface [Fig. 9(c) and 9(f)]. In the center of the dimple, Fe-Cr-O-based oxide particles having a size of several hundred nm and Cr-rich carbide particles having a much coarse diameter of several μm were partially observed. While the dimple cell observed in the high ED PBF sample's fracture surface had a relatively small diameter of hundreds of nm, the wrought specimens, which showed a typical ductile deformation, had relatively large and deep dimples of around 4 μm.

On the other hand, the heat-treated DED specimens did not show a cup-and-cone shape fracture and localized necking, and thus fine dimples of around 1μm were evenly distributed on the fracture surface. In general, the fracture surface of AM specimens is microscopically very smooth like a brittle transgranular fracture surface, and the dimple cell is much smaller than that of their conventionally built counterparts. Sometimes pinhole-like large and deep defects were observed on the fracture surface, and the presence of these defects under the condition of lack of ductility was expected to reduce the mechanical properties of AM samples significantly.

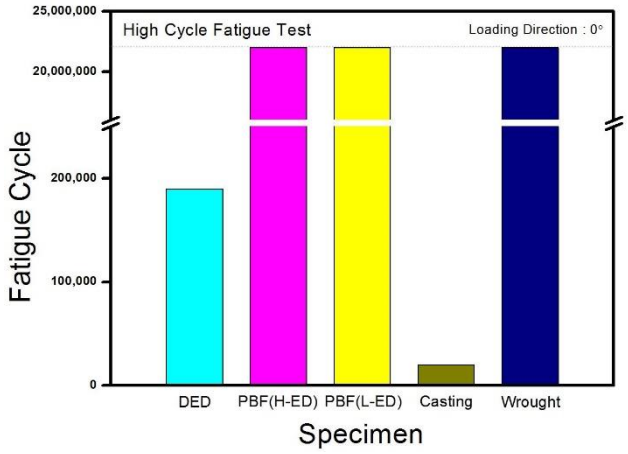

Fig. 11. Comparison of the high cycle fatigue life for 316L SS specimens taken from the standard components after heat treatment.

Sharpy impact tests showed that the impact strength of metal AM parts was more than 75% lower than wrought specimens (Fig. 10). Impact strength is thought to be having a direct linear relationship with elongation rate (EL), and therefore it is necessary to improve the ductility to strengthen the impact characteristics sufficiently. Besides, homogenized heat treatment showed a distinct effect of improving impact strength in all test specimens. The findings show that the most critical point for the AM process is how to secure sufficient ductility, rather than having a high strength. Fatigue characteristics also appeared to be significantly affected by ductility. When a fatigue test is conducted on a round-shaped specimen, the fatigue life varies greatly depending on whether the fatigue load exceeds the yield strength of each test specimen. In this fatigue test, the fatigue load was in the range of 30 to 300 MPa, so the fatigue life was extremely short in casting, and DED samples whose yield strength was lower than 300 MPa (Fig. 11). The remaining specimens had a yield strength of 590 MPa or more, so no fractures occurred in all coupons over 2 million fatigue cycles

IV. Conclusion

In this paper, the characterization of microstructure and mechanical properties of metal AM coupons have been performed. Based on the achieved results, the following conclusions can be drawn:

1) Metal AM parts are superior to parts manufactured by conventional processes such as casting and wrought in terms of strength but have a poor impact and fatigue properties due to low ductility, which is the characteristics of the rapid cooling process.

2) Thorough attention is required to manage the metal nanoparticles as it may not melt well due to oxidation of the powder surface or agglomeration between particles by reacting with moisture or oxygen in the atmosphere.

3) Low energy density may introduce incomplete melting of metal powder, and consequently, the large-sized lack of fusion pore can be formed. On the contrary, if the energy density is too high, the ductility is reduced significantly by forming a non-equilibrium martensitic microstructure with a high density of dislocation.

4) The low ED PBF samples exhibit satisfactory mechanical properties comparable to wrought specimens in terms of impact and fatigue characteristics known to be most vulnerable in metal AM samples. Therefore, it is expected to be used well in the electric power sector requiring high reliability if AM process parameters, beam strategies, and post-heat treatment conditions are fully optimized.

Acknowledgment

This work is supported by Korea Electric Power Corporation under Grant R16XA05.

References

[1] W.E. Frazier, “Metal additive manufacturing: a review,” J. Mater. Eng. Perform. 23 (2014) 1917-1928, https://doi.org/10.1007/s11665-014-0958-z.

[2] D.D. Gu, W. Meiners, K. Wissenbach, R. Poprawe, “Laser additive manufacturing of metallic components: materials, processes and mechanisms,” Int. Mater. Rev. 57 (2012) 133-164, https://doi.org/10.1179/1743280411Y.0000000014.

[3] T.J. Hensen, T.G. Aguirre, C.L. Cramer, A.S. Wand, K. Ma, D.A. Prawel, J. D. Williams, T.B. Holland, “Additive manufacturing of ceramic nanopowder by direct coagulation printing,” Addit. Manuf. 23 (2018) 140-150, https://doi.org/ 10.1016/j.addma.2018.07.010.

[4] W.J. Sames, F.A. List, S. Pannala, R.R. Dehoff, S.S. Babu, “The metallurgy and processing science of metal additive manufacturing,” Int. Mater. Rev. 1 (2016) 315-360, https://doi.org/10.1080/09506608.2015.1116649.

[5] A. Uriondo, M. Esperon-Miguez, S. Perinpanayagam, “The present and future of additive manufacturing in the aerospace sector: a review of important aspects,” Proc. Inst. Mech. Eng. Part G J. Aerosp. Eng. 229 (2015) 2132-2147, https://doi. org/10.1177/0954410014568797.

[6] G. Marchese, S. Parizia, M. Rashidi, A. Saboori, D. Manfredi, D. Ugues, M. Lombardi, E. Hryha, S. Biamino, “The role of texturing and microstructure evolution on the tensile behavior of heat-treated Inconel 625 produced via laser powder bed fusion,” Mater. Sci. Eng. A769 (2020) 138500, https://doi.org/10.1016/ j.msea.2019.138500.

[7] K. Zhang, S. Wang, W. Liu, X. Shang, “Characterization of stainless steel parts by laser metal deposition shaping,” Mater. Des. 55 (2014) 104-119, https://doi.org/10.1016/j.matdes.2013.09.006.

[8] M. Ziętala, T. Durejko, M. Polański, I. Kunce, T. Płociński, W. Zieliński, M. Łazińska, W. Stępniowski, T. Czujko, K.J. Kurzydłowski, Z. Bojar, “The microstructure, mechanical properties and corrosion resistance of 316 L stainless steel fabricated using laser engineered net shaping,” Mater. Sci. Eng. A677 (2016) 1-10, https://doi.org/10.1016/j.msea.2016.09.028.

[9] K. Saeidi, X. Gao, Y. Zhong, Z.J. Shen, “Hardened austenite steel with columnar subgrain structure formed by laser melting,” Mater. Sci. Eng. A625 (2015) 221-229, ttp://dx.doi.org/10.1016/j.msea.2014.12.018.

[10] H. Gong, K. Rafi, H. Gu, T. Starr, B. Stucker, “Analysis of defect generation in Ti–6Al–4V parts made using powder bed fusion additive manufacturing processes,” Addit. Manuf. 1–4 (2014) 87-98, http://dx.doi.org/10.1016/j.addma.2014.08.002.

[11] A.S. Wu, D.W. Brown, M. Kumar, G.F. Gallegos, W.E. King, “An experimental investigation into additive manufacturing-induced residual stresses in 316L stainless steel,” Metall. Mater. Trans. A45 (2014) 6260-6270, https://doi.org/10.1007/s11661-014-2549-x.

[12] S. Leuders, M. Thöne, A. Riemer, T. Niendorf, T. Tröster, H.A. Richard, H.J. Maier, “On the mechanical behaviour of titanium alloy TiAl6V4 manufactured by selective laser melting: fatigue resistance and crack growth performance,” Int. J. Fatigue 48 (2013) 300-307, https://doi.org/10.1016/j.ijfatigue.2012.11.011.

[13] H.K. Rafi, N.V. Karthik, H. Gong, T.L. Starr, B.E. Stucker, “Microstructures and mechanical properties of Ti6Al4V parts fabricated by selective

laser melting and electron beam melting," J. Mater. Eng. Perform. 22 (12) (2013) 3872-3883, https://doi.org/10.1007/s11665-013-0658-0.

[14] X. Chen, J. Li, X. Cheng, B. He, H. Wang, Z. Huang, "Microstructure and mechanical properties of the austenitic stainless steel 316L fabricated by gas metal arc additive manufacturing," Mater. Sci. Eng. A703 (2017) 567-577, https://doi.org/10.1016/j.msea.2017.05.024.

[15] T. Ronneberg, C. M. Davies, P. A. Hooper, "Revealing relationships between porosity, microstructure and mechanical properties of laser powder bed fusion 316L stainless steel through heat treatment," Mater. Des. 189 (2020) 108481, https://doi.org/10.1016/j.matdes.2020.108481.